Ionic Mechanisms for Intrinsic Slow Oscillations in Thalamic Relay Neurons

A. Destexhe,*‡ A. Babloyantz,‡ and T. J. Sejnowski*

*The Howard Hughes Medical Institute and The Salk Institute, Computational Neurobiology Laboratory, La Jolla, California 92037 USA; and ‡Université Libre de Bruxelles, CP 231 Campus Plaine, Boulevard du Triomphe, B-1050 Bruxelles, Belgium

ABSTRACT The oscillatory properties of single thalamocortical neurons were investigated by using a Hodgkin-Huxley-like model that included Ca^{2+} diffusion, the low-threshold Ca^{2+} current (I_T) and the hyperpolarization-activated inward current (I_h). I_h was modeled by double activation kinetics regulated by intracellular Ca^{2+}. The model exhibited waxing and waning oscillations consisting of 1–25-s bursts of slow oscillations (3.5–4 Hz) separated by long silent periods (4–20 s). During the oscillatory phase, the entry of Ca^{2+} progressively shifted the activation function of I_h, terminating the oscillations. A similar type of waxing and waning oscillation was also observed, in the absence of Ca^{2+} regulation of I_h, from the combination of I_T, I_h, and a slow K^+ current. Singular approximation showed that for both models, the activation variables of I_h controlled the dynamics of thalamocortical cells. Dynamical analysis of the system in a phase plane diagram showed that waxing and waning oscillations arose when I_h entrained the system alternately between stationary and oscillating branches.

INTRODUCTION

The thalamus is central to the generation of oscillatory activity during slow wave sleep. Two types of rhythmical activities of the electroencephalogram have been characterized, spindle waves (7–14 Hz) and delta waves (0.5–4 Hz). Spindle waves depend on both intrinsic and network mechanisms in the thalamus (Steriade and Deschenes, 1984; Steriade and Llinas, 1988). Until recently (Steriade et al., 1990) delta waves were assumed to originate in the cortex. However, a recent study conducted in cat in vivo (Curró Dossi et al., 1992; Nunez et al., 1992) showed that the thalamus can generate spontaneous oscillations of 0.5–4 Hz even after severing its connections with the cortex, which suggests an important thalamic contribution in the genesis of delta waves.

In vitro experiments on thalamocortical (TC) cells have demonstrated an intrinsic low-threshold Ca^{2+} spike (Jahnsen and Llinas, 1984a) and a tendency to oscillate. Cat and rat TC neurons display spontaneous slow oscillations in the delta range (Haby et al., 1988; Leresche et al., 1990, 1991; McCormick and Pape, 1990a) which are resistant to tetrodotoxin and therefore due to mechanisms intrinsic to the cell. These slow oscillations have also been called "pacemaker oscillations" (Leresche et al., 1990, 1991).

A waxing and waning oscillation was also found in cat TC cells in vitro (Leresche et al., 1990, 1991). These oscillations are composed of periods of 1.5–28 s of 0.5–3.2-Hz oscillation that wax and wane, separated by silent phases of 5–25-s duration. They are resistant to tetrodotoxin and are caused by mechanisms intrinsic to the TC neuron. By analogy with the

waxing and waning of in vivo spindles, they have been called "spindle-like oscillation" (Leresche et al., 1990, 1991). However in vivo spindles occur at a higher intraburst frequency (7–14 Hz) and depend on interactions with neurons of the thalamic reticular nucleus (Steriade and Deschenes, 1984; Steriade et al., 1985, 1987, 1990), so they are quite different from the waxing and waning slow oscillations studied here.

Electrophysiological investigations of the ionic mechanisms responsible for the intrinsic properties of TC neurons have revealed the presence of a low-threshold Ca^{2+} current, I_T, responsible for the generation of low-threshold spikes (LTS) following hyperpolarization (Deschenes et al., 1984; Jahnsen and Llinas, 1984b). More recently, voltage-clamp studies of this current in TC cells (Coulter et al., 1989; Crunelli et al., 1989; Huguenard and Prince, 1992) characterized the kinetic properties of I_T and the characteristic activation of this current in the subthreshold region of the membrane potential.

A mixed Na^+/K^+ current, I_h, responsible for anomalous rectification, has also been identified in TC neurons studied in vitro (McCormick and Pape, 1990a; Pollard and Crunelli, 1988). The voltage-clamp technique has revealed that I_h is activated by hyperpolarization in the subthreshold range of potentials (McCormick and Pape, 1990a; Soltesz et al., 1991). This current was also shown to be involved in the generation of the slow oscillations of TC neurons (McCormick and Pape, 1990a; Soltesz et al., 1991) as well as in the state control of TC neurons by several neuromodulatory systems (McCormick and Pape, 1990a; McCormick and Williamson, 1991; Pape, 1992). The regulation of I_h can also control the transition between slow oscillations and waxing and waning oscillations in cat TC cells (Soltesz et al., 1991).

The purpose of the present paper is to investigate possible ionic mechanisms underlying the waxing and waning oscillations observed in single TC cells in vitro using a model of the TC neuron. The kinetic mechanisms in the model are

based on voltage-clamp data of I_T and I_h. Special emphasis is given to uncovering the role of I_h in organizing the transitions between multiple oscillatory and resting states of the TC cell.

MATERIALS AND METHODS

Our single compartment model of a TC cell used a Hodgkin-Huxley-type scheme (Hodgkin and Huxley, 1952) for the ionic currents. The equation describing the derivative of the membrane potential V was:

$$C_m \dot{V} = -g_L(V - E_L) - I_T - I_h - I_{K2} + I_{ext}, \qquad (1)$$

where $C_m = 1$ $\mu F/cm^2$ is the specific capacity of the membrane, $g_L = 0.05$ mS/cm^2, and $E_L = -86$ mV are, respectively, the leakage conductance and the leakage reversal potential. The value of g_L was chosen to obtain a membrane time constant of 20 ms, and E_L was adjusted to match the resting membrane potential to -60 mV (Jahnsen and Llinas, 1984a) when I_h was present, and to more hyperpolarized levels, when I_h was blocked (McCormick and Pape, 1990b). The total membrane area was assumed to be 1000 μm^2, the area of a typical TC cell soma. Dendrites were not taken into account.

Only currents absolutely necessary to generate subthreshold oscillations were included in the model. These currents were the low-threshold Ca^{2+} current I_T, the hyperpolarization-activated current I_h and the voltage-dependent K$^+$ current I_{K2}. I_{ext} represents the external current applied to the cell. Other Na$^+$ and K$^+$ currents, such as the I_{Na} and I_K responsible for the generation of action potentials, I_A, I_{NaP}, or I_C were not included in the model (for details on these currents see McCormick and Huguenard, 1992).

Kinetic models have been developed previously for I_T (Huguenard and McCormick, 1992; Wang et al., 1991), for I_h (Destexhe and Babloyantz, 1993; Huguenard and McCormick, 1992), and I_{K2} (Huguenard and McCormick, 1992). We use them as our starting point.

The low-threshold Ca^{2+} current I_T

Voltage-clamp experiments (Coulter et al., 1989; Crunelli et al., 1989) show that the dynamical properties of I_T can be accounted for by a Hodgkin-Huxley-type formalism. A four-variable model of this low-threshold current was recently proposed by Wang et al. (1991) and will be used here. The kinetic equations read:

$$I_T = -\bar{g}_{Ca} m^3 h (V - E_{Ca})$$

$$\dot{m} = -\frac{1}{\tau_m(V)}[m - m_\infty(V)]$$

$$\dot{h} = \alpha_1(V)[1 - h - d - K(V)h] \qquad (2)$$

$$\dot{d} = \alpha_2(V)[K(V)(1 - h - d) - d],$$

where $\bar{g}_{Ca} = 1.75$ mS/cm^2 is the maximum value of the conductance of the Ca^{2+} current and E_{Ca} is the Ca^{2+} reversal potential (in the presence of Ca^{2+} diffusion, E_{Ca} was calculated from the Nernst relation, and was taken as $E_{Ca} = 120$ mV otherwise). In this kinetic scheme, m is the activation and h and d are two inactivation variables. The variable d accounts for the slow recovery of I_T from inactivation (Wang et al., 1991). The various functions used here are listed in Table 1.
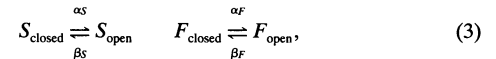
The hyperpolarization activated current I_h

Voltage-clamp studies on thalamocortical neurons (McCormick and Pape, 1990a; Soltesz et al., 1991) have shown that I_h is a noninactivating current that activates slowly. This current is carried by both Na$^+$ and K$^+$ ions, and its reversal potential lies between E_{Na} and E_K (McCormick and Pape, 1990a). I_h activates in the same subthreshold range of membrane potentials as I_T.

TABLE 1 Activation functions and time constants for the voltage-dependent currents I_T, I_h, and I_{K2}.

Current	Variable	Function
I_T	m	$m_\infty(V) = 1/\{1 + \exp[-(V + 65)/7.8]\}$
		$\tau_m(V) = 0.15 m_\infty(V)\{1.7 + \exp[-(V + 30.8)/13.5]\}$
	h	$\alpha_1(V) = \exp[-(V + 162.3)/17.8]/0.26$
		$K(V) = \sqrt{0.25 + \exp[(V + 85.5)/6.3]} - 0.5$
	d	$\alpha_2(V) = 1/\{\tau_2(V)[K(V) + 1]\}$
		$\tau_2(V) = 62.4/\{1 + \exp[(V + 39.4)/30]\}$
I_h	S_1, F_1	$H_\infty(V) = 1/\{1 + \exp[(V + 68.9)/6.5]\}$
	S_1	$\tau_S(V) = \exp[(V + 183.6)/15.24]$
		$\tau_F(V) = \exp[(V + 158.6)/11.2]/$
	F_1	$\{1 + \exp[(V + 75)/5.5]\}$
I_{K2}	$m2$	$m_{2\infty(V)} = 1/\{1 + \exp -[(V + 43)/17]\}$
		$\tau_{m2}(V) = 2.86 + 0.29/\{\exp[(V - 81)/25.6]$
		$+ \exp[-(V + 132)/18]\}$
	h_1, h_2	$h_{2\infty}(V) = 1/\{1 + \exp[(V + 58)/10.6]\}$
	h_1	$\tau_{h1}(V) = 34.65 + 0.29/\{\exp[(V - 1329)/200]$
		$+ \exp[-(V + 130)/7.1]\}$
	h_2	$\tau_{h2}(V) = \tau_{h1}(V) \quad$ for $\quad V \geq -70$ mV
		$\tau_{h2}(V) = 2570$ ms $\quad$ for $\quad V < -70$ mV

These functions were chosen to fit voltage-clamp measurements of these currents. All values were scaled to a temperature of 36°C assuming Q_{10} values of 5 and 3 for I_T (Coulter et al., 1989), and of 2.6 for I_{K2} (Huguenard and Prince, 1991). The screening charge effect was calculated assuming an extracellular Ca^{2+} concentration of 2 mM.

Recently, a kinetic scheme for I_h was introduced to account for the kinetic properties of I_h (Destexhe and Babloyantz, 1993). Two distinct activation gates were assumed, namely F (fast activation) and S (slow activation) according to the following kinetic scheme:

$$S_{closed} \underset{\beta_S}{\overset{\alpha_S}{\rightleftharpoons}} S_{open} \qquad F_{closed} \underset{\beta_F}{\overset{\alpha_F}{\rightleftharpoons}} F_{open}, \qquad (3)$$

where S_{closed} and F_{closed} represent the closed states of the slow and fast activation gates of I_h, S_{open} and F_{open} represent the open states of these gates, and α_S, β_S, α_F, and β_F are voltage-dependent rate constants (see below). The corresponding kinetic equations are:

$$I_h = \bar{g}_h S_1 F_1 (V - E_h)$$

$$\dot{S}_1 = \alpha_S(V)S_0 - \beta_S(V)S_1 \qquad (4)$$

$$\dot{F}_1 = \alpha_F(V)F_0 - \beta_F(V)F_1,$$

where $\bar{g}_h$ is the maximal conductance of I_h (in mS/cm^2), $E_h = -43$ mV is the reversal potential of I_h (McCormick and Pape, 1990a), $S_0 = 1 - S_1$, and $F_0 = 1 - F_1$. S_0 and F_0 represent the fraction of activation gates in the closed state, whereas S_1 and F_1 are the fraction of activation gates in the open state. The conductance of I_h is always proportional to the product $S_1 F_1$ in this model.
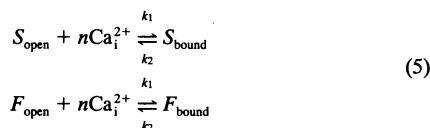
The rate constants are related to the activation function $H_\infty(V)$ and the time constants $\tau_S(V)$ and $\tau_F(V)$ by the following relations: $\alpha_S = H_\infty/\tau_S$, $\beta_S = (1 - H_\infty)/\tau_S$, $\alpha_F = H_\infty/\tau_F$ and $\beta_F = (1 - H_\infty)/\tau_F$. The activation function $H_\infty(V)$ was chosen so that H_∞^2 fit the data of McCormick and Pape (1990a) (see Table 1). The time constants $\tau_F(V)$ and $\tau_S(V)$ (given in Table 1) were estimated from numerical simulation of voltage-clamp protocols (see Results).

Regulation of I_h by intracellular Ca^{2+}

Two plausible ionic mechanisms which produce waxing and waning oscillatory behavior are presented in Results. One possibility, initially pro-

posed by McCormick (1992), is the regulation of I_h by binding of intracellular Ca^{2+}, as found in whole cell voltage-clamp studies of I_h in sino-atrial node cells (Hagiwara and Irisawa, 1989). Evidence for the control of the voltage-dependent properties of I_h by intracellular Ca^{2+} were also obtained in cat neocortical neurons (Schwindt et al., 1992). As the Ca^{2+} dependence of I_h has not yet been studied in TC cells, it was assumed to be similar to that of sino-atrial node cells.

The activation curve of I_h in sino-atrial node cells shifts toward more positive potentials as the intracellular Ca^{2+} concentration ($[Ca]_i$) is increased (Hagiwara and Irisawa, 1989). Calmodulin and protein kinase C were not involved in the Ca^{2+} modulation of I_h, suggesting that Ca^{2+} ions directly affected I_h channels (Hagiwara and Irisawa, 1989). There is also an increase of the conductance of I_h following the binding of Ca^{2+}. We have developed a kinetic model for intracellular calcium (Ca_i^{2+}) binding to the open channels of I_h that is consistent with these data. The open state gates S_{open} and F_{open} were assumed to have n binding sites for Ca_i^{2+} which, when occupied, lead to the open forms S_{bound} and F_{bound} according to:

$$S_{open} + nCa_i^{2+} \underset{k_2}{\overset{k_1}{\rightleftharpoons}} S_{bound}$$
$$F_{open} + nCa_i^{2+} \underset{k_2}{\overset{k_1}{\rightleftharpoons}} F_{bound} \quad (5)$$

where k_1 and k_2 are the forward and backward rate constants for Ca_i^{2+} binding.

If S_2 and F_2 represent the fraction of gates bound to calcium, then, combining Eqs. 3 and 5, one obtains the following kinetic equations for I_h:

$$I_h = \bar{g}_h(S_1 + S_2)(F_1 + F_2)(V - E_h)$$
$$\dot{S}_1 = \alpha_S(V)S_0 - \beta_S(V)S_1 + k_2[S_2 - CS_1]$$
$$\dot{F}_1 = \alpha_F(V)F_0 - \beta_F(V)F_1 + k_2[F_2 - CS_1] \quad (6)$$
$$\dot{S}_2 = -k_2[S_2 - CS_1]$$
$$\dot{F}_2 = -k_2[F_2 - CF_1],$$

where $S_0 = 1 - S_1 - S_2$, $F_0 = 1 - F_1 - F_2$, $C = ([Ca]_i/Ca_{crit})^n$, and α_S, β_S, α_F, and β_F were obtained from H_∞ and τ_S as before. The number of binding sites was $n = 2$ in all of our simulations. We assumed $k_1 = k_2/Ca_{crit}^n = 5 \times 10^{-4}$ mM is the critical value of $[Ca]_i$ at which Ca^{2+} binding on I_h channels is half-activated (if $[Ca]_i \ll Ca_{crit}$, the effect of Ca_i^{2+} is negligible; see Results for the estimation of this parameter from voltage-clamp data). $k_2 = 4 \times 10^{-4}$ ms^{-1} is the inverse of the time constant of Ca_i^{2+} binding on I_h channels. These values were chosen to match the slow time course with which I_h is modulated by intracellular Ca^{2+}.

Influx and efflux of Ca^{2+}

The dynamics of intracellular Ca^{2+} were determined by two contributions:

(i) Influx of Ca^{2+} due to I_T

Ca^{2+} ions enter through I_T channels and diffuse into the interior of the cell. Only the Ca^{2+} concentration in a thin shell beneath the membrane was modeled. The influx of Ca^{2+} into such a thin shell followed:

$$[Ca]_i = -\frac{k}{2Fd}I_T, \quad (7)$$

where $F = 96489$ C mol^{-1} is the Faraday constant, $d = 1$ μm is the depth of the shell beneath the membrane, and the unit conversion constant is $k = 0.1$ for I_T in μA/cm$_2$ and $[Ca]_i$ in millimolar.

(ii) Efflux of Ca^{2+} due to an active pump

In a thin shell beneath the membrane, Ca^{2+} retrieval usually consists of a combination of several processes, such as binding to Ca^{2+} buffers, calcium

efflux due to Ca^{2+} ATPase pump activity and diffusion to neighboring shells. Only the Ca^{2+} pump was modeled here. We adopted the following kinetic scheme:

$$Ca_i^{2+} + P \underset{c_2}{\overset{c_1}{\rightleftharpoons}} CaP \overset{c_3}{\rightarrow} P + Ca_o^{2+}, \quad (8)$$
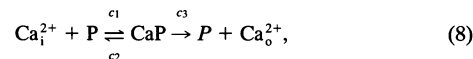
where P represents the Ca^{2+} pump, CaP is an intermediate state, Ca_o^{2+} is the extracellular Ca^{2+} concentration, and c_1, c_2, and c_3 are rate constants. Ca^{2+} ions have a high affinity for the pump P, whereas extrusion of Ca^{2+} follows a slower process (Blaustein, 1988). Therefore, c_3 is low compared to c_1 and c_2, and the Michaelis-Menten approximation can be used for describing the kinetics of the pump. According to such a scheme, the kinetic equation for the Ca^{2+} pump is:

$$[Ca]_i = -\frac{K_T[Ca]_i}{[Ca]_i + K_d}, \quad (9)$$

where $K_T = 10^{-4}$ mM ms^{-1} is the product of c_3 with the total concentration of P, and $K_d = c_2/c_1 = 10^{-4}$ mM is the dissociation constant, which can be interpreted here as the value of $[Ca]_i$ at which the pump is half activated (if $[Ca]_i \ll K_d$ then the efflux is negligible).

The parameters of the pump were adjusted in order to have a fast Ca^{2+} removal, based on an estimation made from the time course of the spike after hyperpolarization in TC cells (McCormick and Huguenard, 1992). Slow Ca^{2+} handling is unlikely since Ca^{2+}-dependent channels would detect a slow Ca^{2+} accumulation in TC cells.

The extracellular Ca^{2+} concentration was $[Ca]_o = 2$ mM as found in vivo. The change of $[Ca]_i$ due to the binding of Ca^{2+} to I_h channels was negligible and was neglected, as was the contribution of Ca^{2+} efflux to the net Ca^{2+} current in Eq. 7.

The Ca^{2+} reversal potential strongly depends on the intracellular Ca^{2+} concentration, and was calculated according to the Nernst relation:

$$E_{Ca} = k'\frac{RT}{2F}\log\frac{[Ca]_o}{[Ca]_i}, \quad (10)$$

where $R = 8.31$ J mol^{-1} K^{-1}, $T = 309°$ K, and the constant for unit conversion is $k' = 1000$ for E_{Ca} in mV. For $[Ca]_i = 2.4 \times 10^{-4}$ mM, which is an average value at rest in the simulations presented here, E_{Ca} was approximately 120 mV.

Slow K^+ current I_{K2}

A second plausible ionic mechanism for the generation of waxing and waning oscillations depends on the interaction between three ionic currents, namely I_T, I_h, and a slow outward current. Different types of K^+ currents have been recently identified in TC cells (Budde et al., 1992; Huguenard and Prince, 1991; McCormick, 1991). Among these, a slowly inactivating K^+ current activated by depolarization was characterized and termed I_{K2} by Huguenard and Prince (1991). They reported that this current inactivates very slowly with two time constants (around 250 ms and 3 s). A very similar current was found in TC cells in the lateral geniculate nucleus (McCormick, 1991). A kinetic model for this current was proposed by Huguenard and McCormick (1992):

$$I_{K2} = \bar{g}_{K2}m_2(0.6h_1 + 0.4h_2)(V - E_K)$$
$$\dot{m}_2 = -\frac{1}{\tau_{m2}(V)}(m_2 - m_{2\infty(V)})$$
$$\dot{h}_1 = -\frac{1}{\tau_{h1}(V)}(h_1 - h_{2\infty(V)}) \quad (11)$$
$$\dot{h}_2 = -\frac{1}{\tau_{h2}(V)}(h_2 - h_{2\infty(V)})$$

where $\bar{g}_{K2}$ is the maximum value of I_{K2} conductance and $E_K = -90$ mV is the reversal potential for K^+ ions. The activation function and the time constant of the activation variables m_2, h_1, and h_2 are given in Table 1.

Estimation of the values of parameters

Conductances values and reversal potentials for the above currents were estimated from published values provided by measurements in vitro. However, these data only provide approximate values for these parameters. Also, the complex dendritic geometry of the cell was not taken into account, which would affect these values. For each of the currents considered here, the value of the maximal conductance and the reversal potential are interrelated. For example, if E_h is increased, $\bar{g}_h$ must be decreased to reproduce similar results. We tested a broad range of maximal conductances and similar results were obtained.

Methods for solving the equations

Exploration of the behavior of the system over a large range of values of the parameters was performed using programs developed specifically for the purpose of this paper, or by using the NEURON simulator (Hines, 1989, 1993). The solutions were obtained by direct integration of the differential equations using a fifth order, variable-step integration subroutine, provided by the CERN library (MERSON D208: accuracy of 10^{-3}–10^{-5}%, minimal step reached 10^{-1}–10^{-3} ms). These solutions were rigorously identical to those obtained from the NEURON simulator (Euler integration, minimal step of 10^{-1}–10^{-2} ms).

The stationary states of the system (see Results) were calculated analytically, and the equations obtained were solved numerically by using a Newton-Raphson algorithm (Press et al., 1986). A confirmation of the value of the stationary state was also provided by direct integration of the differential equations.

The programs written for the purpose of this paper and the NEURON simulator were run on UNIX workstations (SONY NWS 3410 and MIPS 3000), and the typical time taken by a simulation of 10 s was of the order of 8–16 s CPU time.

RESULTS

TC cells exhibit several types of slowly oscillating states in the subthreshold range of potentials (−60 to −80 mV). These oscillations were based on interactions between subthreshold currents, such as the low threshold Ca^{2+} current I_T and the hyperpolarization-activated current I_h. In particular, the mechanisms proposed here depend strongly on the kinetic properties of I_h. The parameters for I_h in our model were adjusted to fit voltage-clamp data.

Ca^{2+} and voltage-dependent activation of I_h

The activation function of I_h at equilibrium as a function of the membrane potential and the intracellular Ca^{2+} concentration is, from Eq. 6:

$$H_\infty(V, [Ca]_i) = [(S_1 + S_2)(F_1 + F_2)]_{eq}$$

$$= \left[\frac{1 + C}{H_\infty(V)^{-1} + C} \right]^2, \qquad (12)$$

where $C = ([Ca]_i/Ca_{crit})^n$, $H_\infty(V)^2 = H_\infty(V, [Ca]_i = 0)$. The activation function $H_\infty(V, [Ca]_i)$ was determined from voltage-clamp measurements of TC neurons (McCormick and Pape, 1990a), and the parameters of $H_\infty(V)$ were chosen to fit as closely as possible these data (Fig. 1 B, solid line).

Whole cell voltage-clamp experiments (Hagiwara and Irisawa, 1989) on sino-atrial node cells have shown that increasing intracellular Ca^{2+} produces a shift of the activation
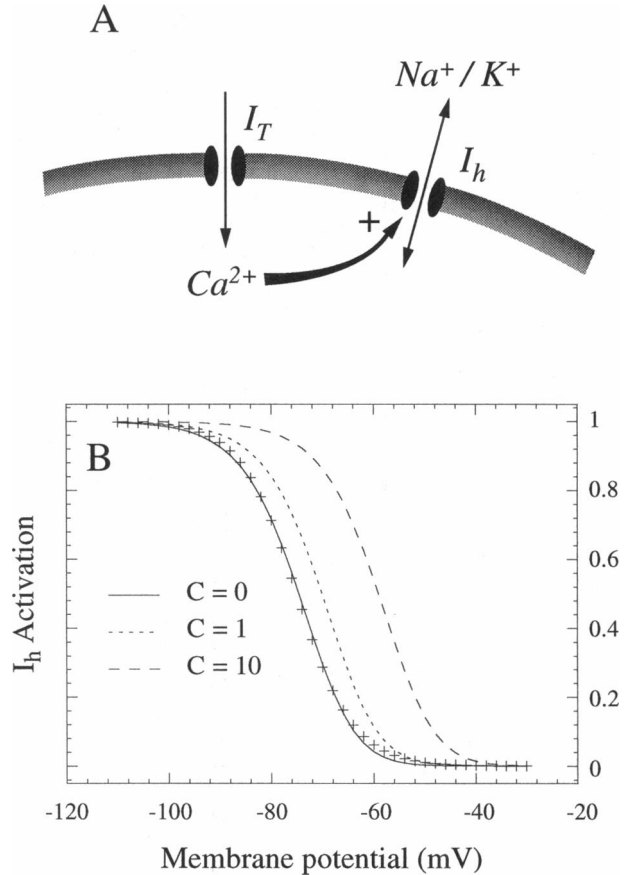

A

FIGURE 1 Ca^{2+}-induced shift of the activation function of I_h. (A) Schematic diagram illustrating the currents in the model. The low-threshold Ca^{2+} current (I_T) lets Ca^{2+} ions enter the cell; these ions bind to the mixed Na^+/K^+ channel I_h and modify its voltage-dependent properties. (B) Direct binding of intracellular Ca^{2+} to I_h channels shifts the voltage dependence of the current toward positive membrane potentials. $H_\infty(V, [Ca_i])$ is represented as a function of the membrane potential V for different values of $[Ca]_i$. The activation function at resting level of $[Ca]_i$ (solid line: $C = 0$) was estimated from voltage-clamp experiments (McCormick and Pape, 1990a) on TC cells (+ symbols). For increasing concentrations of intracellular Ca^{2+}, the activation function shows progressively larger shifts toward positive membrane potential (dashed lines, $C = 1$ and $C = 10$). $C = ([Ca]_i/Ca_{crit})^2$.

function of I_h toward more positive membrane potentials. Using patch pipettes containing various concentrations in Ca^{2+}, the shift was around 13 mV for the highest concentrations in Ca^{2+} used.

These data can be accounted for by a kinetic scheme where intracellular Ca^{2+} directly binds to the I_h channels (see Fig. 1 A and Materials and Methods). The activation function $H_\infty(V, [Ca]_i)$ progressively shifts toward positive membrane potentials as the value of C increases (Fig. 1 B).

The shift at half-activation of I_h is obtained by substituting $H_\infty(V, [Ca]_i) = 0.5$ into Eq. 12, to obtain:

$$V_{1/2} = -68.9 + 6.5[\log(\sqrt{2} - 1) \log(C + 1)]$$

$$\simeq -75 + 6.5 \log\left[\left(\frac{[Ca]_i}{Ca_{crit}} \right)^n + 1 \right]. \qquad (13)$$

The shift of the I_h activation logarithmic in $[Ca]_i$ and a shift of 13 mV is obtained for $C = 6.4$.

The shift should be negligible ($C < 1$) at the resting level, $[Ca]_i \sim 2 \times 10^{-4}$ mM, which gives a lower bound: $Ca_{crit} > 2 \times 10^{-4}$ mM. During activation of I_T, the value of $[Ca]_i$ just beneath the membrane increases to about 10^{-2}–10^{-3} mM and shifts I_h by a few millivolts ($C > 1$), which gives an upper bound: $Ca_{crit} < 10^{-2}$–10^{-3} mM. In the simulations presented here, we chose $n = 2$ and $Ca_{crit} = 5 \; 10^{-4}$ mM.

Kinetics of I_h

I_h activates very slowly and its time constant can be greater than 1 s at 3–6°C (McCormick and Pape, 1990a; Soltesz et al., 1991). The time course of I_h activation may differ considerably from the time course of deactivation at the same membrane potential. Currents similar to I_h in other preparations also show very slow activation and, in some cases, a faster time course for deactivation (for recent studies on I_h, see Erickson et al., 1993; Galligan et al., 1990; Kamondi and Reiner, 1991; Uchimura et al., 1990; van Ginneken and Giles, 1991; and references therein).

Despite the different time constants for activation and deactivation, I_h follows a single exponential time course, which would suggest a simple description involving first order kinetics. However, in a simple first-order kinetic scheme, the time constant of activation is identical to that of deactivation.

A novel kinetic scheme was proposed (Destexhe and Babloyantz, 1993) to account for these apparently conflicting experimental data (see Materials and Method). We assume that the permeability of I_h channels depends on two independent gates (S for slow activation and F for fast activation) which must be opened simultaneously.

This model exhibits two time constants. Following a depolarizing voltage jump, the two gates S and F, which are initially closed, begin to activate: the fast variable F_1 rapidly increases to its equilibrium value, whereas S_1 reaches the same value more slowly. Since I_h is proportional to the product $S_1 F_1$, the time course of the measured current will reflect the activation kinetics of the slow variable S_1 (Fig. 2 A). The opposite occurs upon a hyperpolarizing voltage jump from a depolarized level where both gates were initially open: F_1 rapidly closes, while S_1 closes more slowly. Since the decrease of F_1 immediately decreases I_h, the time course of deactivation follows the kinetics of the fast variable (Fig. 2 B).

Although in our model for I_h the current is a product of two exponentials (Eq. 4), the two time constants were sufficiently different that the time course of the current was practically a single exponential. This could explain the single exponential curves observed from voltage-clamp experiments of I_h.

The slow time constant, $\tau_S(V)$, was chosen by an exponential fit of voltage-clamp measurements of the time constants of activation, whereas the fast time constant,

$\tau_F(V)$, was fit by a bell-shaped function from measurements of the deactivation time constants (see Fig. 2 C and Table 1).

Simulation of voltage-clamp experiments using these functions produced curves and measurements indistinguishable from those obtained by McCormick and Pape (1990a) (Fig. 2 C). In particular, the double activation scheme for I_h deactivates faster than it activates (Destexhe and Babloyantz, 1993).

In the next section, regulation of I_h by Ca^{2+} is introduced and its interactions with other currents examined.

Oscillatory behavior from Ca^{2+}-regulated I_h

Previous models of TC cells have shown that the interaction between I_T and I_h supports slow oscillations in the delta range 0.5–4 Hz (Lytton and Sejnowski, 1992; McCormick and Huguenard, 1992; Toth and Crunelli, 1992a). We demonstrate here that this slow oscillation can wax and wane as a result of the interaction between the two subthreshold currents I_T and I_h, and the regulation of I_h by intracellular Ca^{2+}.

The double activation model of I_h combined with I_T can give rise to a variety of resting states and slow oscillations. These patterns were obtained for different values of the maximal conductance $\bar{g}_h$ of I_h (Fig. 3). For the lowest values of $\bar{g}_h$ (< 0.01 mS/cm^2), the model remained in a hyperpolarized resting state at about -84 mV (Fig. 3 A). A similar hyperpolarized resting state has been observed in vitro (McCormick and Pape, 1990a; Soltesz et al., 1991) after blockage of I_h.
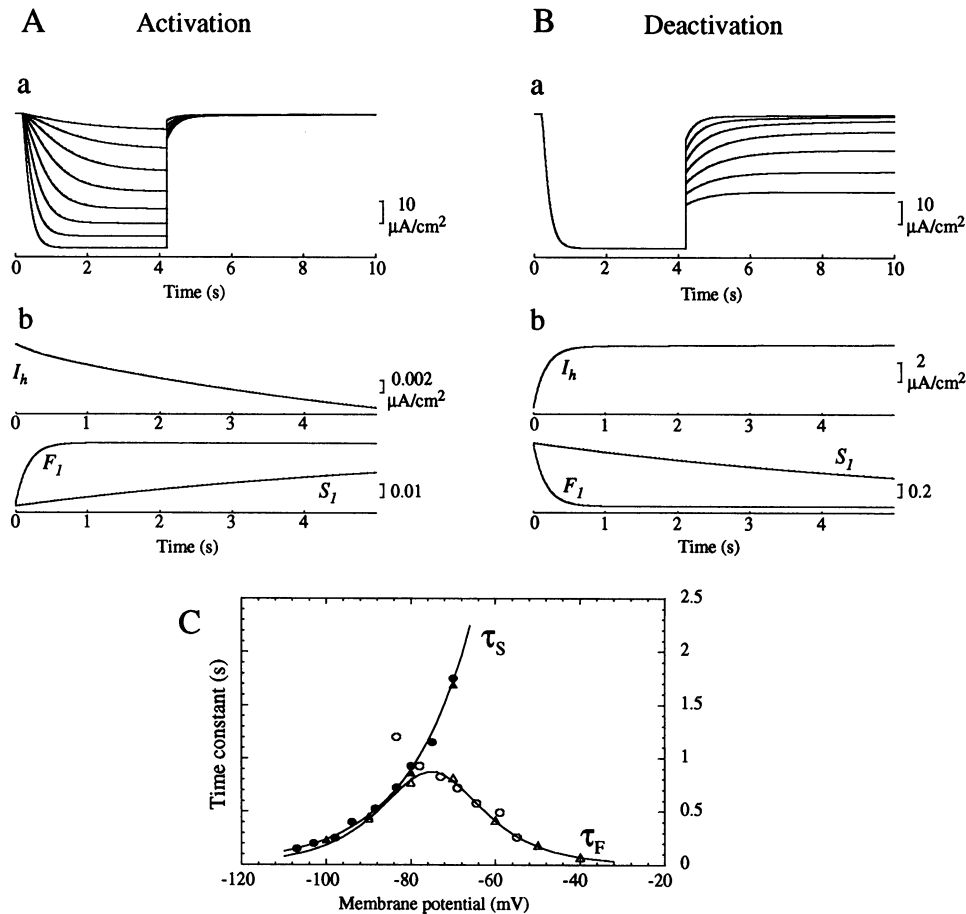
For the highest values of this conductance ($\bar{g}_h > 0.1$mS/cm^2), there was a more depolarized resting state (around -58 mV) close to firing threshold (Fig. 3 D). The depolarized resting state was similar to that observed in vitro following the enhancement of I_h by noradrenaline and probably corresponds to the "relay state" of TC neurons (McCormick and Pape, 1990a; Soltesz et al., 1991).

For moderate values of $\bar{g}_h$, various types of slow oscillatory behavior were observed. In the range of $\bar{g}_h$ between 0.0018 and 0.02 mS/cm^2, there was a regular slow oscillation of 0.5–3.5 Hz (Fig. 3 B) similar to the slow oscillatory behavior recorded in TC cells in vitro (McCormick and Pape, 1990a).

For somewhat higher values of $\bar{g}_h$ (between about 0.02 and 0.09 mS/cm^2), waxing and waning oscillations appeared (Fig. 3 C) that consisted of bursts of slow oscillations (typically lasting a few seconds at frequency of 3.5–4 Hz with faster components at 8–9 Hz) separated by a silent phases lasting about 4–20 s. Such bursts of slow oscillations (0.5–3.2 Hz) separated by silent phases (5–25 s) have been recorded in cat TC cells in vitro (Leresche et al., 1990, 1991).

Properties of Ca^{2+}-dependent waxing and waning oscillations

Soltesz et al. (1991) showed that slow oscillations and waxing and waning oscillations observed in cat TC cells are two

A   Activation

a

B   Deactivation

a

] 10 $\mu A/cm^2$

] 10 $\mu A/cm^2$

b

I_h

] 0.002 $\mu A/cm^2$

F_1 S_1] 0.01

Time (s)

b

I_h] 2 $\mu A/cm^2$

S_1

F_1] 0.2

Time (s)

C

τ_S

τ_F

Time constant (s)

Membrane potential (mV)

FIGURE 2   Activation and deactivation kinetics of I_h. (A) Simulation of voltage-clamp protocols of activation of I_h. (a) From an initial holding value of −55 mV, the voltage was clamped at various levels (from −105 to −70 mV) for 4 s, then clamped again to −55 mV. (b) Time course of the current compared to the gating variables. During this activation protocol (initial voltage of −30 mV, current recorded after clamping to −50 mV at $t = 0$) the current follows the time course of the slow variable S_1. A time constant of about 3 s was estimated from fitting a single exponential to the current trace. (B) Simulation of protocols of deactivation of I_h. (a) The voltage was clamped at −105 mV for 4 s, then clamped to various levels from −85 to −55 mV. (b) Time course of the current and gating variables. In this case, although the voltage was clamped to the same value as in Ab (initial voltage of −110 mV and clamp to −50 mV at $t = 0$), the current followed the time course of the variable F_1 and a smaller time constant of about 180 ms was measured. (C) Time constants for activation and deactivation of I_h as a function of the membrane potential. The time constants obtained by single-exponential fitting of the currents illustrated above for activation (*filled triangles*) and deactivation (*open triangles*) were compared to the measurements obtained by McCormick and Pape (1990a) during activation (*filled circles*) and deactivation (*open circles*). Solid lines represent the functions fit to these data (given in Table 1). Adapted from Destexhe and Babloyantz (1993).

states in a continuum and that the transition from slow oscillations to waxing and waning type of rhythmicity could be achieved by enhancement of I_h. The same sequence of oscillations was observed here as I_h was enhanced in the model (Fig. 3). Other properties of in vitro waxing and waning oscillations include a characteristic hyperpolarization during the silent phase and their transformation into slow oscillations by a depolarizing current step. These properties were also present is our model (Fig. 4, A and B).

The transition from waxing and waning oscillation to slow oscillations from a depolarizing current step was not observed for all values of $\bar{g}_h$. For some values of $\bar{g}_h$, the opposite was observed: waxing and waning oscillations were transformed into slow oscillations by applying a hyperpolarizing current step (not shown).

There was a progressive hyperpolarization during the silent phase (Fig. 4 B). During the burst there was a gradual

depolarization that was most clearly seen by averaging the membrane potential (Fig. 4 C).

The time courses of the different variables of the model during a waxing and waning sequence are displayed in Fig. 5. The membrane hyperpolarized slowly during the silent phase until I_T deinactivated and the oscillations began. During the burst of slow oscillations, Ca^{2+} entered transiently at the peak of each spike and bound progressively to I_h channels (reflected in the slow increase of S_2 and F_2). Ca^{2+} binding to I_h channels shifted the I_h activation curve, producing a gradual depolarization during the oscillatory phase (Fig. 4 C). This depolarization prevented I_T from activating and damped the slow oscillations. During the ensuing silent phase, S_2 and F_2 slowly decreased and caused the membrane to hyperpolarize.

The progressive transformation of slow oscillations into waxing and waning oscillations is shown in Fig. 6. A bifur-

FIGURE 3   Resting states and slow oscillations in the presence of I_T and Ca^{2+}-dependent I_h obtained at four values of the maximal conductance of I_h. (A) Hyperpolarized resting state close to -84 mV for $\bar{g}_h = 0$. (B) Slow oscillations of about 3.5 Hz for $\bar{g}_h = 0.01$ mS/cm². (C) Waxing and waning oscillations of about 4–8 Hz for $\bar{g}_h = 0.04$ mS/cm². (D) Depolarized resting state around -58 mV for $\bar{g}_h = 0.11$ mS/cm². The maximum conductance of I_T was kept fixed at $\bar{g}_{Ca} = 1.75$ mS/cm².
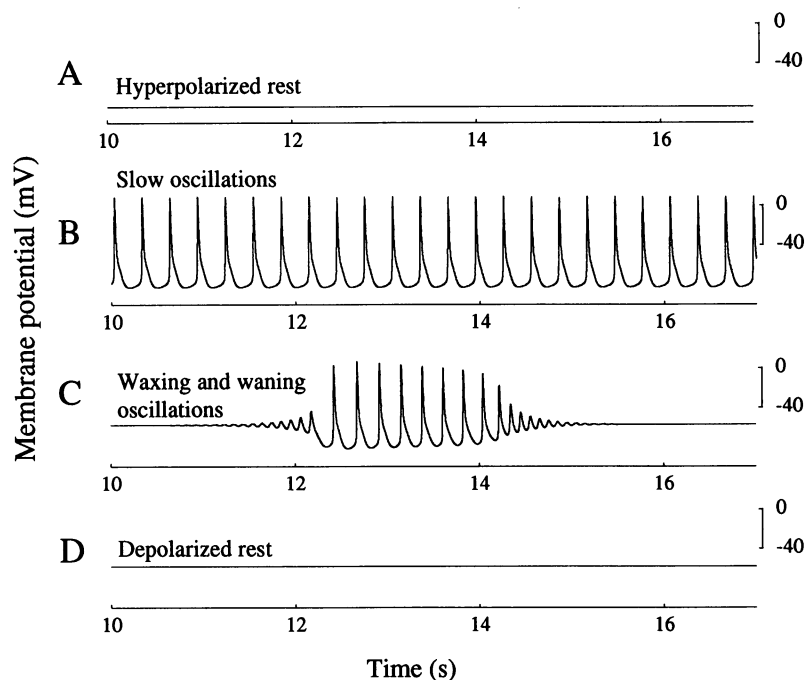
cation occurred around $\bar{g}_h = 0.02$ mS/cm² from slow oscillations to a state where the slow oscillations were interrupted by short silent phases (Fig. 6 B). As $\bar{g}_h$ increased, the length of the silent phase increased and the bursts became shorter (Fig. 6, C and D). The frequency inside the oscillatory phase was always comparable to that of the slow oscillations.

The duration of the silent phase and the oscillatory phase as a function of $\bar{g}_h$ are reported in Fig. 7 A. The silent phase ranged from 4 to 20 s and decreased with $\bar{g}_h$. The oscillatory phase became shorter with increase of $\bar{g}_h$. In the limit, as $\bar{g}_h$ decreased to 0.02 mS/cm², the duration of oscillatory phase tended to infinity. The opposite oc-

curred as the depolarized state was approached, with oscillatory phase reducing to a minimum length before disappearing (sometimes a low amplitude periodic oscillation was seen in a very narrow range of $\bar{g}_h$ before the depolarized state appeared). The period of the slow oscillation decreased with $\bar{g}_h$ (indicated by S in Fig. 7 A), which is consistent with the slowing down of the slow oscillation observed after progressive blockage of I_h channels by cesium (McCormick and Pape, 1990a).

The length of the silent phase and of the oscillatory phase were directly proportional to the time constant of intracellular Ca^{2+} binding to I_h channels, k_2^{-1} (Fig. 7 B). This is

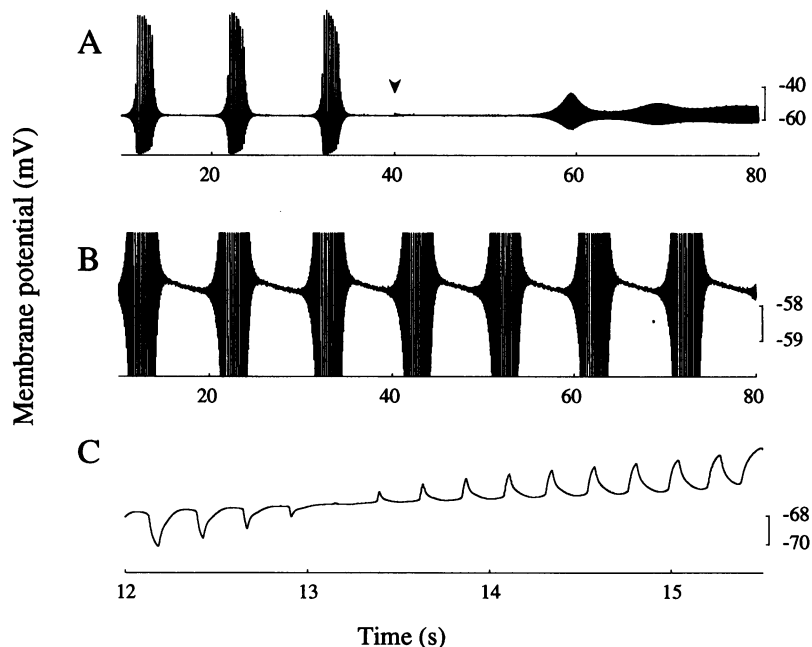FIGURE 4   Properties of Ca^{2+}-dependent waxing and waning oscillations. (A) Transformation of waxing and waning oscillations into slow oscillations by application of a depolarizing current step of 0.05 μA/cm² (arrow). $\bar{g}_h = 0.04$ mS/cm². (B) Waxing and waning oscillations at high amplification showing the slow hyperpolarization of the membrane during the silent phase. $\bar{g}_h = 0.04$ mS/cm². (C) Average membrane potential showing a progressive depolarization during the oscillatory phase. Each point was obtained by averaging the membrane potential over a period of 500 ms. $\bar{g}_h = 0.025$ mS/cm².

consistent with the assumption that the binding of Ca^{2+} is critical for the onset and termination of the oscillatory phase. The silent phase, which depends on the return of S_2 and F_2 to their resting values, is expected to be proportional to k_2^{-1}. The length of the oscillatory phase, which depends on the rate of rise of S_2 and F_2, is also expected to be proportional to k_2^{-1}.

I_{K2}-dependent waxing and waning oscillations

The Ca^{2+}-dependent regulation of I_h is not the only way to obtain waxing and waning oscillation with I_T and I_h. A second possible mechanism depends on the interaction among I_T, I_h, and the slow K^+ current I_{K2}. Ca^{2+} mechanisms were not included in this version of the model.

It was reported previously (Destexhe and Babloyantz, 1993) that the double activation model of I_h showed the same sequence of oscillatory states as in vitro experiments when combined with I_T and I_{K2}. This model was explored using different values for some of the parameters. Characteristic properties of waxing and waning oscillations, such as the progressive hyperpolarization during the silent phase and the transformation into slow oscillations by applying a depolarizing current step, were also observed is this model (Fig. 8).

Fig. 9 shows the time course of several gating variables during a waxing and waning sequence. As in the mechanism proposed by Soltesz et al. (1991), I_h activates more and more

during each cycle of the oscillatory phase. The resulting depolarization inactivates I_T and the oscillations damp.

Compared with the Ca^{2+}-dependent waxing and waning oscillations, the slow depolarization of the membrane during the oscillatory phase in the I_{K2}-dependent model is provided by a more pronounced I_h activation (S_1 reaches its maximal value during the oscillatory phase) and inactivation of I_{K2}. Progressive deactivation of I_h then hyperpolarizes the membrane.

Waxing and waning oscillations were never observed without adding a slow depolarization-activated outward current in addition to I_T and I_h. Similar oscillations were observed when I_{K2} was replaced by slow K^+ currents, such as the slow Ca^{2+}-activated K^+ current or a depolarization-activated noninactivating K^+ current similar to the muscarinic current I_M (not shown). However, these currents are probably not present in TC cells.

Singular approximation of waxing and waning oscillations

Instead of studying the mechanisms of waxing and waning oscillations in terms of activation variables and Ca^{2+} concentration, it is possible to describe these oscillations as *dynamical states* of the system. This provides a more global view of "stationary states" or "limit cycle oscillations" of the system. Complex oscillatory processes, such as oscillations
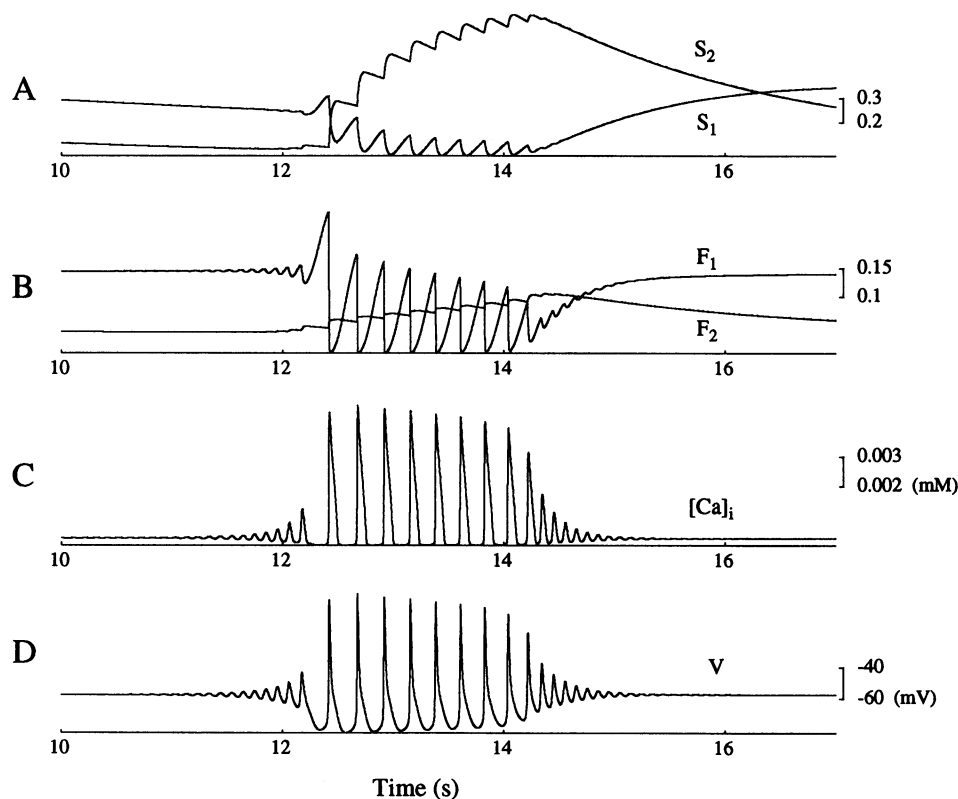

FIGURE 5 Time course of the gating variables of I_h during Ca^{2+}-dependent waxing and waning oscillations. (A) Slow activation variables S_1 and S_2. (B) Fast activation variables F_1 and F_2. (C) Intracellular Ca^{2+} concentration $[Ca]_i$. (D) Membrane potential V. $\bar{g}_h$ = 0.04 mS/cm^2. Same parameters as in Fig. 3 C.
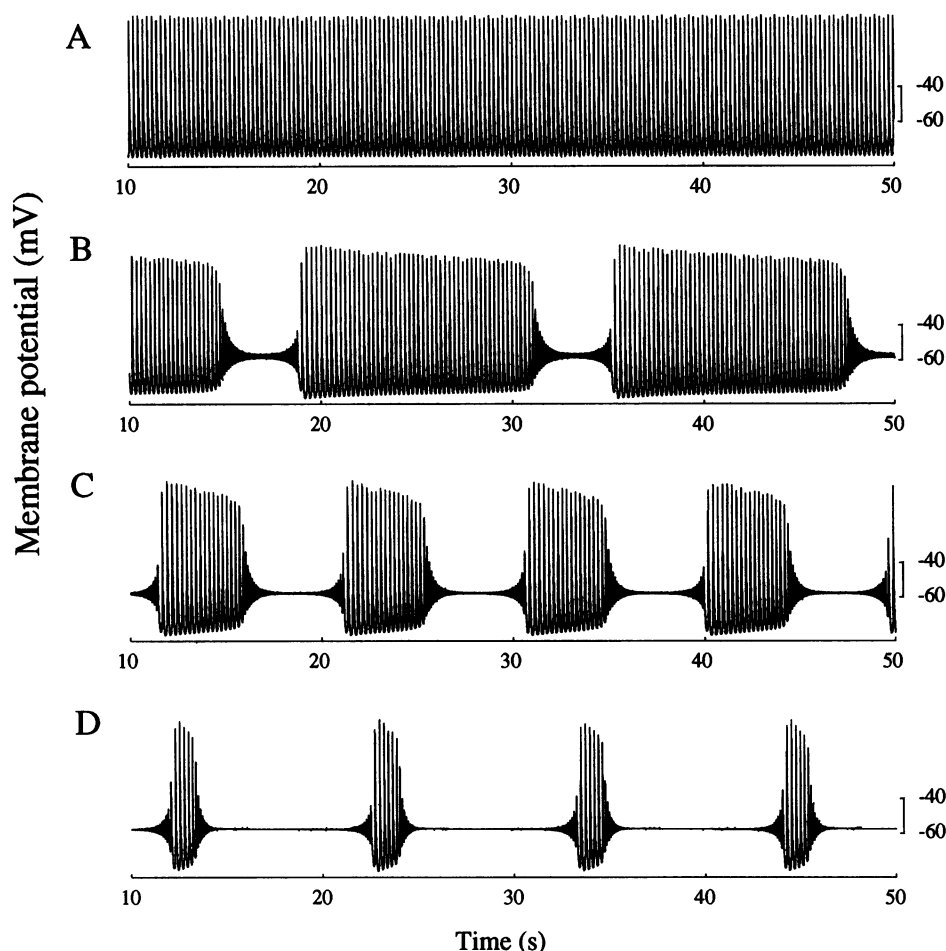
FIGURE 6   Transformation from slow oscillations to waxing and waning oscillations. The pattern of oscillations is shown for four values of $\bar{g}_h$. (A) slow oscillations ($\bar{g}_h$ = 0.02 mS/cm^2). (B) A short silent phase interrupted the slow oscillation ($\bar{g}_h$ = 0.021 mS/cm^2). (C) Oscillations with a longer silent phase ($\bar{g}_h$ = 0.025 mS/cm^2). (D) For larger values of $\bar{g}_h$, the silent phase became more prominent ($\bar{g}_h$ = 0.05 mS/cm^2).

that wax and wane, usually result from several oscillatory or stationary states. In this section, the dynamical states underlying waxing and waning oscillations are studied using a singular approximation method that identifies the origin and the transitions between these states.

Singular approximation is used in nonlinear dynamics to separate fast and slow subsystems (Pontryagin, 1961; Zeeman, 1973). Slow variables can be treated as slowly varying parameters and the rest of the system can then be studied as a function of these new parameters. This approximation has been successfully used to uncover the dynamical mechanisms underlying bursting oscillations in models of several biological systems (Rinzel, 1987).

We have applied this method to our model of waxing and waning oscillations. In Fig. 5, the gating variables S_2 and F_2 evolved according to a slower time scale than the other variables. In the case of I_{K2}-dependent waxing and waning oscillations (Fig. 9), S_1 and h_2 were the slow variables.

Let S_2 be a slowly varying parameter in the Ca^{2+}-dependent model. In contrast, F_2 only displays small variations of amplitude and therefore has a less prominent role

than S_2. As before, Eq. 6 was used for Ca^{2+}-dependent waxing and waning oscillations, except that S_2 was assigned a constant value. In Fig. 5 A, since the variable S_2 oscillates approximately between 0.09 and 0.65, the same interval of values will be used for S_2 treated as a parameter.

Over this range of values, the system showed either a stable resting state or limit cycle oscillations (Fig. 10 A). For the smallest values of S_2, the system exhibited slow oscillations at a frequency of about 3.5 Hz, whereas for the highest values of the parameter S_2, the system exhibited a stable stationary state close to the depolarized resting state of Fig. 3 (around −57 mV).

The transition point between limit cycle oscillations and stable stationary state is called a *Hopf bifurcation* (Guckenheimer and Holmes, 1986; Rinzel and Ermentrout, 1989). In some cases, the stable solutions overlap, and the bifurcation is called *subcritical*. In our system, this transition has the typical structure of a subcritical Hopf bifurcation. First, the amplitude of the limit cycle at the bifurcation point changed abruptly and there was no decline in amplitude. Second, in some range of values of the parameter S_2 (about 0.225–0.42),
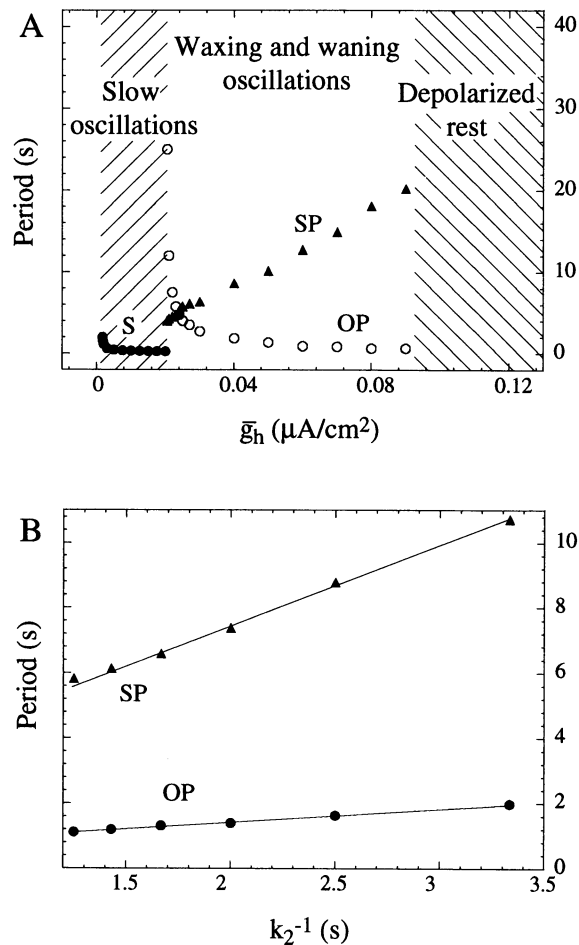
FIGURE 7   The period of Ca^{2+}-dependent waxing and waning oscillations depends on the maximal conductance of I_h and the time constant of Ca^{2+} binding to I_h channels. The length of the silent phase (SP) and the length of the oscillatory phase (OP) are shown as a function of these two parameters. (A) Period as a function of the maximal conductance of I_h ($\bar{g}_h$). The range of values of $\bar{g}_h$ corresponding to slow oscillations (period labeled by S), waxing and waning oscillations and depolarized resting state are also indicated. (B) Period as a function of the time constant (k_2^{-1}) of intracellular Ca^{2+} binding on I_h channels. The inverse of the rate k_2 is the time constant for Ca^{2+} binding.

the stable limit cycle coexisted with the stable stationary state (Fig. 10 B). The state of the system within this interval of S_2 depended on its previous history.

Thus, in a waxing and waning sequence, S_2 oscillates between values which drive the system alternately between stable stationary states and slow oscillations. As shown by Fig. 10 B, the waxing and waning oscillations are driven around a hysteresis loop by the slow oscillations of S_2, as depicted by dotted arrows: as S_2 decreases during the silent phase, the membrane potential hyperpolarizes slowly and follows the stable stationary state branch (*arrow 1*). As the critical point is reached, the stationary state loses its stability and the system jumps to the oscillating branch (*arrow 2*). S_2 then starts to increase and follows the oscillating branch, while the amplitude of the oscillations decreases (*arrow 3*). The limit cycle oscillations lose stability and the system jumps back to the stationary branch (*arrow 4*). The oscillations damp and the silent phase starts again.

The trajectory of a simulated waxing and waning oscillation plotted in a V/S_2 diagram, shown in Fig. 10 D, alternates between an oscillating and a stationary branch in a manner very similar to that in Fig. 10 B. The position of the oscillating and stationary branches seems to be slightly different from the solutions displayed in Fig. 10 B, but the structure remains the same. Waxing and waning oscillations with a longer oscillatory phase (see Fig. 6) correspond to a very similar trajectory, with an increased number of loops near the end of the oscillatory branch.

The same subcritical Hopf structure is still present for slow oscillations, but the successive loops do not leave the oscillatory branch and the oscillation does not wax and wane. A strong current pulse should, however, be able to make the trajectory jump from the oscillatory branch to the stationary branch. This prediction is borne out in Fig. 11, where a strong depolarizing current step induced a sudden transition to a silent phase during the slow oscillation (indicated by *arrows 2 and 3* in Fig. 11 B) and the system returned back to the oscillatory branch (*arrow 4*) along a single hysteresis loop. Steps applied to S_2 resulted in the same type of behavior.

FIGURE 8   Properties of I_{K2}-dependent waxing and waning oscillations. (A) Transformation of waxing and waning oscillations into slow oscillations by applying a depolarizing current step of 0.24 $\mu A/cm_2$ (*arrow*). (B) Waxing and waning oscillations at high amplification shows the slow hyperpolarization of the membrane during the silent phase. $\bar{g}_h$ = 0.4 mS/cm^2, $\bar{g}_{Ca}$ = 1.75 mS/cm^2.
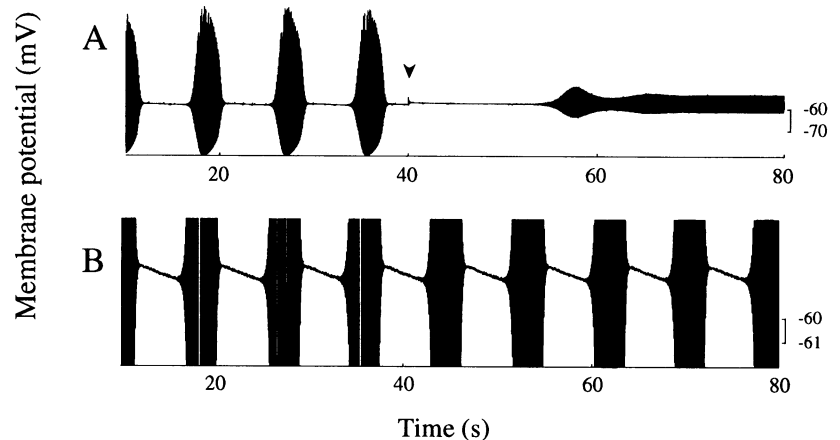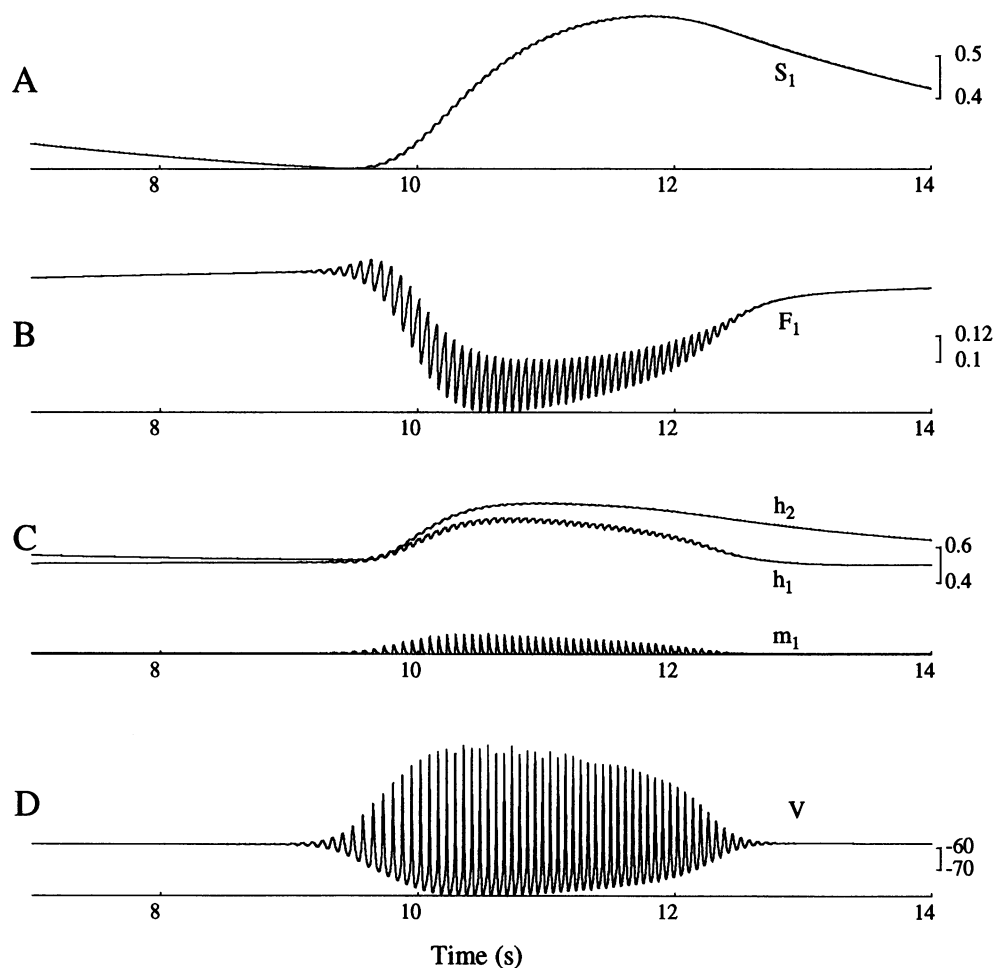
FIGURE 9   Time course of the gating variables of I_h and I_{K2} and the membrane potential during an I_{K2}-dependent waxing and waning oscillation. (A) Slow activation variable S_1 of I_h. (B) Fast activation variable F_1 of I_h. (C) Activation (m_2) and inactivation (h_1, h_2) variables of I_{K2}. (D) Membrane potential V. $\bar{g}_h$ = 0.4 mS/cm^2.

The same analysis can be applied to the I_{K2}-dependent waxing and waning oscillations, using S_1 as a parameter. The I_{K2}-dependent waxing and waning oscillations were also based on a hysteresis loop around a subcritical Hopf bifurcation (not shown). The trajectory in the V/S_2 diagram was very similar to the Ca^{2+}-dependent waxing and waning oscillations (Fig. 12).

DISCUSSION

Hodgkin-Huxley-type models of TC neurons were first introduced by McMullen and Ly (1988) and Rose and Hindmarsh (1989) based on the experiments of Jahnsen and Llinas (1984a). More recent models of TC neurons (Destexhe and Babloyantz, 1993; Lytton and Sejnowski, 1992; McCormick and Huguenard, 1992; Toth and Crunelli, 1992a) take into account data from voltage-clamp experiments. We have extended these models by incorporating a more accurate model of I_h and have used it to study the genesis of waxing and waning oscillations that have been described in vitro (Leresche et al., 1990, 1991; Soltesz et al., 1991).

The properties of I_h in voltage-clamp mode

The hyperpolarization-activated inward current I_h is central to the oscillatory properties of TC neurons (McCormick and Pape, 1990a; Soltesz et al., 1991). First-order kinetic schemes have been proposed for modeling I_h in TC cells (Huguenard and McCormick, 1992; Lytton and Sejnowski, 1992; Toth and Crunelli, 1992a), sino-atrial node cells (DiFrancesco and Noble, 1985; vanGinneken and Giles, 1991) and stomatogastric ganglion neurons (Buchholtz et al., 1992); however, they do not reproduce the slow component of activation and the difference between activation and deactivation kinetics.

The model of I_h adopted here (Destexhe and Babloyantz, 1993) has two activation variables with different kinetics and accurately accounts for all the voltage-clamp data. Although more complex models have been developed for modeling a current similar to I_h in sino-atrial cells (DiFrancesco, 1985), the model used here is relatively simple and explains how slow activation can coexist with faster deactivation.

A Ca^{2+} dependence of I_h was included based on voltage-clamp measurements on sino-atrial node cells (Hagiwara and
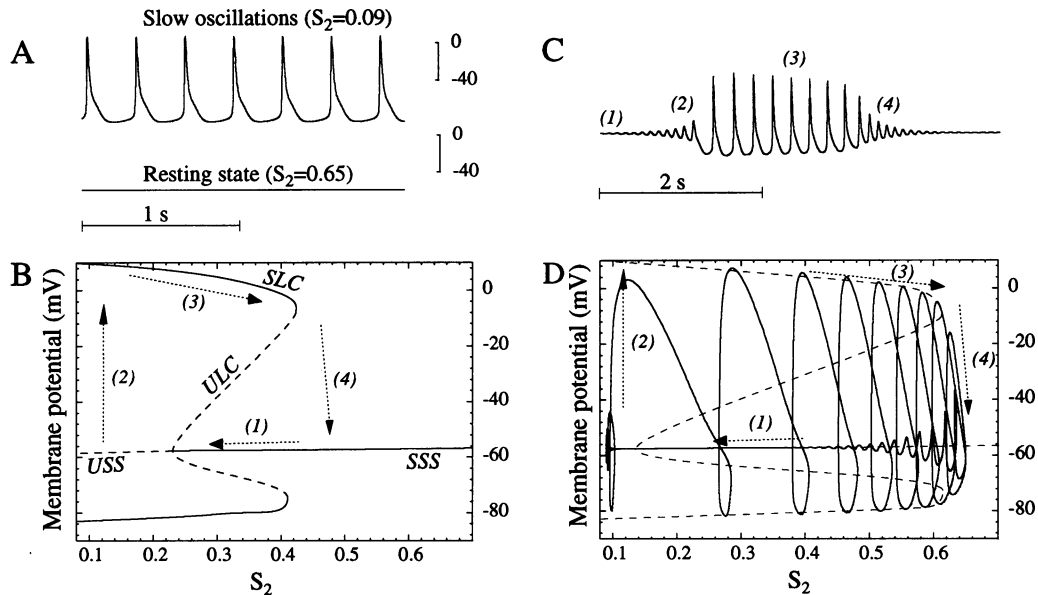
FIGURE 10 Singular approximation applied to the Ca^{2+}-dependent model of waxing and waning oscillations. (*A*) For extreme values of the slow variable S_2 treated as a parameter, the system exhibited either slow oscillations ($S_2 = 0.09$) or a stable stationary state ($S_2 = 0.65$). Other parameters are the same as in Fig. 3 *C*. (*B*) Bifurcation diagram of the system as a function of S_2. During the slow oscillations of S_2, the system alternated between a slow oscillatory state and a resting state, tracing a hysteresis loop as shown in the diagram. The order of events underlying the waxing and waning sequence are indicated by dotted arrows. Dashed lines represent unstable states (*USS*, unstable stationary state; *ULC*, unstable limit cycle), and continuous lines represent stable states (*SSS*, stable stationary state; *SLC*, stable limit cycle). (*C*) Corresponding sequence of events in a single cycle of the waxing and waning oscillations. (*D*) Trajectories of waxing and waning oscillations in the V/S_2 diagram. Here the full system was simulated without considering S_2 as a parameter. Dashed lines represent the presumed position of oscillatory and stationary branches and dotted arrows depict the same sequence of events as in *B*.

Irisawa, 1989) and neocortical neurons (Schwindt et al., 1992). These data suggest that intracellular Ca^{2+} ions directly affect I_h channels and shift the activation function toward more depolarized potentials. We assumed that the Ca^{2+} dependence of I_h is caused by direct binding of Ca^{2+} ions on the open form of I_h channels (for a different model of this shift in the context of TC cells, see Toth and Crunelli (1992b)). Our model accounts for the positive shift of the activation function of I_h with increased intracellular Ca^{2+}, but not for the substantial increase of conductance. It should be possible to verify the predicted logarithmic shift (Eq. 12) from whole cell patch-clamp experiments.

Combinations of currents giving rise to waxing and waning oscillations

The properties of waxing and waning oscillations (Leresche et al., 1991) were reproduced by our model, which included I_T and Ca^{2+}-dependent I_h. The silent phase was many seconds long, during which the membrane potential slowly hyperpolarized. A transition to periodic oscillations could be elicited by application of a depolarizing current step only for some values of the parameter $\bar{g}_h$. Experimental studies report this transition in only two out of 39 cat TC cells (Leresche et al., 1991).

More importantly, the sequence of resting and oscillatory behavior obtained was identical to that determined in vitro (Soltesz et al., 1991). In these experiments, noradrenaline (NE) was used to change I_h, but NE also shifts the activation

function of I_h by a few millivolts (McCormick and Pape, 1990b). We did not include this shift in our simulations.

We also found intermediate patterns of oscillations which were not reported experimentally. Close to the transition between slow oscillations and waxing and waning oscillations there were long oscillatory phases and short silent phases. TC cells in vitro show a variety of patterns of waxing and waning oscillations with silent and oscillatory phases of different lengths. The range of patterns found in the model for different values of the parameters suggests that the variability observed in vitro might arise from a heterogeneity of the conductance values among neurons.

We also investigated the occurrence of waxing and waning oscillations in a model comprising I_T, I_h, and the slow K^+ current I_{K2} (Destexhe and Babloyantz, 1993). The main difference was that the frequency inside the oscillatory phase was significantly higher in I_{K2}-dependent waxing and waning oscillations (10–14 Hz) compared to the same oscillations obtained from the Ca^{2+}-dependent mechanism (3.5–4 Hz). The frequency of oscillations in the Ca^{2+}-dependent model was much closer to the experimental data of Leresche et al. (1991).

In the case of the Ca^{2+}-dependent model, the waxing and waning oscillations were modulated by the kinetics of binding of Ca^{2+}, whereas, in the case of the I_{K2}-dependent model, they appear to be modulated by the slow activation of I_h. Although the values of I_T and leakage parameters were the same, 10-fold higher values of $\bar{g}_h$ were needed to observe similar types of behavior for the I_{K2}-dependent model.
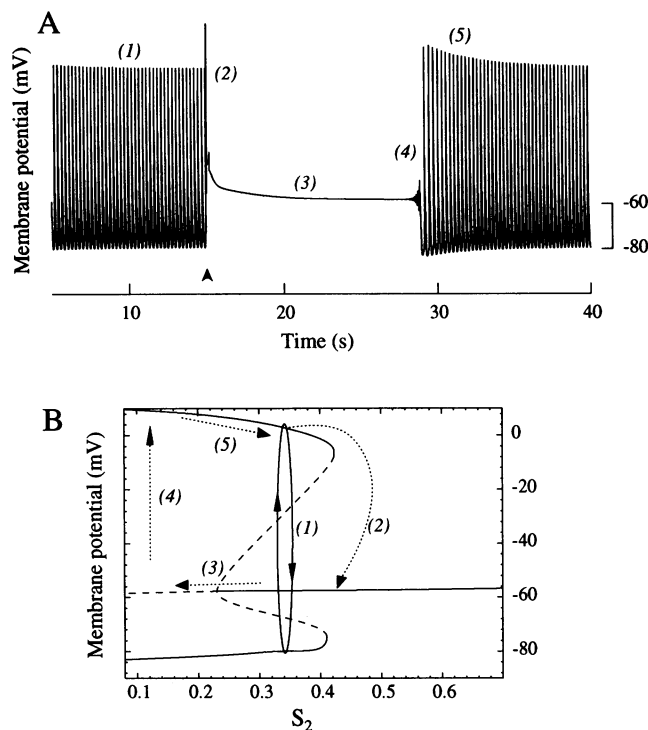
FIGURE 11   Induction of a silent phase during slow oscillations. (A) A strong depolarizing current pulse of 200 ms and 10 μA/cm^2 (0.1 nA) (arrow) damps the slow oscillation for several seconds until spontaneously reappearing. Same parameters as in Fig. 6 A. (B) Same sequence of events illustrated in a V/S_2 diagram. The stable and unstable branches are as described in Fig. 10 B; the closed curve (1) represents the slow oscillation limit cycle and the dotted arrows (2–5) indicate the sequence of events induced by the current pulse. The same sequence of events is reported in A.

Ca^{2+}-dependent waxing and waning oscillations were also observed in the presence of fast Na$^+$ and K$^+$ currents responsible for action potentials (unpublished; kinetics taken from Traub and Miles (1991)). In this case, waxing and waning oscillations occurred as sequences of rhythmic bursting (3.5–4 Hz; fast spikes at 50–300 Hz) separated by long silent phases (4–30 s).

Dynamical mechanisms of waxing and waning oscillations

Singular approximation was used to characterize the waxing and waning oscillation as an alternation between two dynamical states, a hyperpolarizing stationary phase and an oscillating phase. The transitions between these two states were made via a subcritical Hopf bifurcation. It was remarkable that the same dynamical mechanism underlies both the Ca^{2+}-dependent and the I_{K2}-dependent models, despite the different ionic mechanisms.

A similar type of dynamical mechanism was proposed previously by Rinzel (1987) for the Fitzhugh-Nagumo equations (Fitzhugh, 1961), in which a subcritical Hopf bifurcation emerged from a stationary state, leading to bursting oscillations. The same subcritical Hopf structure was also present during slow oscillations. We found that a strong depolarizing
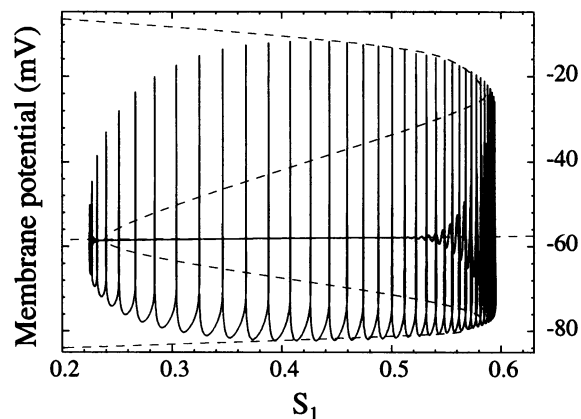
FIGURE 12   Trajectories of waxing and waning oscillations for I_{K2}-dependent waxing and waning oscillations. The same type of diagram as Fig. 10 D is constructed with V plotted against S_1 (same parameters as in Fig. 9). Dashed lines are the presumed positions of oscillatory and stationary branches.

current pulse of 200 ms can force the TC cell out of the oscillatory phase for a period of about 15 s before the cells reverts back to slow oscillations. However, weaker current pulses do not produce such an interruption but only affect the phase of the slow oscillations (not shown). This prediction of the model could be tested experimentally.

The role of I_h

Soltesz et al. (1991) suggested that slow oscillations and waxing and waning rhythmicity observed in vitro correspond to two different equilibria between I_T and I_h. The results presented here are consistent with this hypothesis.

The pattern of oscillations depended on the value of the maximal conductance of I_h and slowly varying this parameter smoothly transforms the slow oscillations into waxing and waning oscillations. This suggests that slow oscillations and waxing and waning oscillations are part of a continuum of oscillating states that can be determined in part by the maximal conductance of I_h.

The Ca^{2+}-dependent waxing and waning oscillations were insensitive to the details of the kinetics of the models for I_T and for the kinetics of binding of intracellular Ca^{2+} on I_h channels. However, when Ca^{2+} binding to I_h was modeled by a simple activation scheme (Huguenard and McCormick, 1992) rather than the double activation model (Destexhe and Babloyantz, 1993), then waxing and waning oscillations were not observed over a wide range of parameter values. These results suggest that the description of I_h by double activation kinetics might be important for robustly generating waxing and waning patterns of oscillation, but more evidence is needed to demonstrate this point.

Implications for the physiology of thalamic oscillations

Our model suggests that interactions between I_T, I_h, and the leakage currents are the kernel that allows the coexistence of

tonic firing, slow oscillations, and waxing and waning oscillations in TC cells. Experiments can be designed to test which of the two proposed mechanisms is responsible for the oscillations. The higher frequency of the I_{K2}-dependent model makes it less plausible than the Ca^{2+}-dependent model. The I_{K2}-dependent model predicts that the waxing and waning oscillations should not survive blockage of all voltage-dependent K^+ currents (but not the leak K^+ currents, needed to maintain the level of membrane potential). The Ca^{2+}-dependent model could be tested by altering the intracellular Ca^{2+} levels while monitoring the period of waxing and waning oscillations. The Ca^{2+}-dependent model predicts that this period should be sensitive to intracellular Ca^{2+}.

The intrinsic oscillating properties of TC cells are difficult to reconcile with the various types of oscillations found in vivo (Nunez et al., 1992). The occurrence of spindling in vivo is thought to be a combination of intrinsic and network properties (Steriade and Llinas, 1988; Steriade et al., 1993b). In particular, single thalamic reticular cells are characterized by 7–12-Hz intrinsic oscillations (Avanzini et al., 1989; Bal and McCormick, 1993), close to the typical frequency of sleep spindles. Spindle rhythmicity was also found in the isolated reticular thalamus in vivo (Steriade et al., 1987). On the other hand, TC cells have a clear tendency to oscillate at a lower frequency of 0.5–4 Hz (Curró Dossi et al., 1992; Leresche et al., 1990, 1991; McCormick and Pape, 1990a) and have been shown to have an active role in the generation of spindles in vitro (von Krosigk et al., 1993). Computer models of the intrinsic oscillatory properties of thalamic reticular and TC cells, as well as their pattern of connectivity, could help us to understand the cellular bases of spindling (Destexhe et al., 1993a,b).

REFERENCES

Avanzini, G., M. de Curtis, F. Panzica, and R. Spreafico. 1989. Intrinsic properties of nucleus reticularis thalami neurones of the rat studied in vitro. *J. Physiol. (Lond.).* 416: 111–122.

Bal, T., and D. A. McCormick. 1993. Mechanisms of oscillatory activity in guinea-pig nucleus reticularis thalami in vitro: a mammalian pacemaker. *J. Physiol. (Lond.).* 468:669–691.

Blaustein, M. P. 1988. Calcium transport and buffering in neurons. *Trends Neurosci.* 11:438–443.

Buchholtz, F., J. Golowasch, I. R. Epstein, and E. Marder. 1992. Mathematical model of an identified stomatogastric ganglion neuron. *J. Neurophysiol.* 67:332–340.

Budde, T., R. Mayer, and H. C. Pape. 1992. Different types of potassium outward current in relay neurons acutely isolated from the rat lateral geniculate nucleus. *Eur. J. Neurosci.* 4:708–722.

Coulter, D. A., J. R. Huguenard, and D. A. Prince. 1989. Calcium currents in rat thalamocortical relay neurones: kinetic properties of the transient, low-threshold current. *J. Physiol. (Lond.).* 414:587–604.

Crunelli, V., S. Lightowler, and C. E. Pollard. 1989. A T-type Ca^{2+} current underlies low-threshold Ca^{2+} potentials in cells of the cat and rat lateral geniculate nucleus. *J. Physiol. (Lond.).* 413:543–561.

Curró Dossi, R., A. Nunez, and M. Steriade. 1992. Electrophysiology of a slow (0.5–4 Hz) intrinsic oscillation of cat thalamocortical neurones in vivo. *J. Physiol. (Lond.).* 447:215–234.

Deschênes, M., M. Paradis, J. P. Roy, and M. Steriade. 1984. Electrophysiology of neurons of lateral thalamic nuclei in cat: resting properties and burst discharges. *J. Neurophysiol.* 55:1196–1219.

Destexhe, A., and A. Babloyantz. 1993. A model of the inward current I_h and its possible role in thalamocortical oscillations. *NeuroReport.* 4:223–226.

Destexhe, A., W. W. Lytton, T. J. Sejnowski, D. A. McCormick, D. Contreras, and M. Steriade. 1993a. A model of 7–14 Hz spindling in the thalamus and thalamic reticular nucleus: interaction between intrinsic and network properties. *Soc. Neurosci.* 19:516.

Destexhe, A., D. A. McCormick, and T. J. Sejnowski. 1993b. A model of 8–10 Hz spindling in interconnected thalamic relay and reticularis neurons. *Biophys. J.* In press.

DiFrancesco, D. 1985. The cardiac hyperpolarization-activated current I_f, origins and developments. *Prog. Biophys. Mol. Biol.* 46:163–183.

DiFrancesco, D., and D. Noble. 1985. A model of cardiac electrical activity incorporating ionic pumps and concentration changes. *Philos. Trans. R. Soc. Lond. B Biol. Sci.* 307:353–398.

Erickson, K. R., O. K. Ronnekleiv, and M. J. Kelly. 1993. Electrophysiology of guinea-pig supraoptic neurones: role of a hyperpolarization-activated cation current in phasic firing. *J. Physiol. (Lond.).* 460:407–425.

Fitzhugh, R. 1961. Impulses and physiological states in models of nerve membrane. *Biophys. J.* 1:445–466.

Galligan, J. J., H. Tatsumi, K. Z. Shen, A. Surprenant, and R. A. North. 1990. Cation current activated by hyperpolarization (I_h) in guinea pig enteric neurons. *Am. J. Physiol.* 259:G966–972.

Guckenheimer, J., and P. Holmes. 1986. Nonlinear Oscillations, Dynamical Systems and Bifurcations of Vector Fields. Springer, Berlin. 459 pp.

Haby, M., N. Leresche, D. Jassik-Gerschenfeld, I. Soltesz, and V. Crunelli. 1988. Spontaneous rhythmic depolarizations in projection cells of the rat lateral geniculate nucleus in vitro: role of NMDA receptors. *C. R. Acad. Sci. Paris Ser. III.* 306:195–199.

Hagiwara, N., and H. Irisawa. 1989. Modulation by intracellular Ca^{2+} of the hyperpolarization-activated inward current in rabbit single sino-atrial node cells. *J. Physiol. (Lond.).* 409:121–141.

Hines, M. 1989. A program for simulation of nerve equations with branching geometries. *Int. J. Biomed. Comput.* 24:55–68.

Hines, M. 1993. NEURON—a program for simulation of nerve equations. *In* Neural Systems: Analysis and Modeling. F. Eeckman, editor. Kluwer Academic Publishers. Norwell, MA. 127–136.

Hodgkin, A. L., and A. F. Huxley. 1952. A quantitative description of membrane current and its application to conduction and excitation in nerve. *J. Physiol. (Lond.).* 117:500–544.

Huguenard, J. R., and D. A. McCormick. 1992. Simulation of the currents involved in rhythmic oscillations in thalamic relay neurons. *J. Neurophysiol.* 68:1373–1383.

Huguenard, J. R., and D. A. Prince. 1992a. Slow inactivation of a TEA-sensitive K current in acutely isolated rat thalamic relay neurons. *J. Neurophysiol.* 66:1316–1328.

Huguenard, J. R., and D. A. Prince. 1992b. A novel T-type current underlies prolonged Ca^{2+}-dependent bursts firing in GABAergic neurons of rat thalamic reticular nucleus. *J. Neurosci.* 12:3804–3817.

Jahnsen, H., and R. R. Llinas. 1984a. Electrophysiological properties of guinea-pig thalamic neurons: an in vitro study. *J. Physiol. (Lond.).* 349: 205–226.

Jahnsen, H., and R. R. Llinas. 1984b. Ionic basis for the electroresponsiveness and oscillatory properties of guinea-pig thalamic neurons in vitro. *J. Physiol. (Lond.).* 349:227–247.

Kamondi, A., and P. B. Reiner. 1991. Hyperpolarization-activated inward current in histaminergic tuberomammillary neurons of the rat hypothalamus. *J. Neurophysiol.* 66:1902–1911.

Leresche, N., D. Jassik-Gerschenfeld, M. Haby, I. Soltesz, and V. Crunelli. 1990. Pacemaker-like and other types of spontaneous membrane potential oscillations in thalamocortical cells. *Neurosci. Lett.* 113:72–77.

Leresche, N., S. Lightowler, I. Soltesz, D. Jassik-Gerschenfeld, and V. Crunelli. 1991. Low frequency oscillatory activities intrinsic to rat and cat thalamocortical cells. *J. Physiol. (Lond.).* 441:155–174.

Lytton, W. W., and T. J. Sejnowski. 1992. Computer model of ethosuxi-mide's effect on a thalamic cell. *Ann. Neurol.* 32:131–139.

McCormick, D. A. 1991. Functional properties of a slowly inactivating potassium current in guinea-pig dorsal lateral geniculate relay neurons. *J. Neurophysiol.* 66:1176–1189.

McCormick, D. A. 1992. Neurotransmitter actions in the thalamus and ce-rebral cortex and their role in neuromodulation of thalamocortical ac-tivity. *Prog. Neurobiol.* 39:337–388.

McCormick, D. A., and J. R. Huguenard. 1992. A model of the electro-physiological properties of thalamocortical relay neurons. *J. Neuro-physiol.* 68:1384–1400.

McCormick, D. A., and H. C. Pape. 1990a. Properties of a hyperpolarization-activated cation current and its role in rhythmic oscillations in thalamic relay neurones. *J. Physiol. (Lond.).* 431:291–318.

McCormick, D. A., and H. C. Pape. 1990b. Noradrenergic modulation of a hyperpolarization-activated cation current in thalamic relay neurones. *J. Physiol. (Lond.).* 431:319–342.

McCormick, D. A., and A. Williamson. 1991. Modulation of neuronal firing mode in cat and guinea pig LGNd by histamine: possible cellular mecha-nisms of histaminergic control of arousal. *J. Neurosci.* 11:3188–3199.

McMullen, T. A., and N. Ly. 1988. Model of oscillatory activity in thalamic neurons: role of voltage and calcium-dependent ionic conductances. *Biol. Cybernet.* 58:243–259.

Nunez, A., R. Curro Dossi, D. Contreras, and M. Steriade. 1992. Intracellular evidence for incompatibility between spindle and delta oscillations in thalamocortical neurons of cat. *Neuroscience.* 48:75–85.

Pape, H. C. 1992. Adenosine promote burst activity in guinea-pig genicu-locortical neurones through two different ionic mechanisms. *J. Physiol. (Lond.).* 447:729–753.

Pollard, C. E., and V. Crunelli. 1988. Intrinsic membrane currents in pro-jection cells of the cat and rat lateral geniculate nucleus. *Neurosci. Lett.* 32:S39.

Pontryagin, L. S. 1961. Asymptotic behavior of the solutions of systems of differential equations with a small parameter in the higher derivatives. *Am. Math. Soc. Trans. Sec. II.* 18:275–290.

Press, W. H., B. P. Flannery, S. A. Teukolsky, and W. T. Vetterling. 1986. Numerical Recipes. The Art of Scientific Computing. Cambridge Uni-versity Press, Cambridge. 735 pp.

Rinzel, J. 1987. A formal classification of bursting mechanisms in excitable systems. *In* Mathematical Topics in Population Biology, Morphogenesis and Neurosciences. E. Teramoto and M. Yamaguti, editors. Springer-Verlag, Berlin. 267–281.

Rinzel, J., and G. B. Ermentrout. 1989. Analysis of neural excitability and oscillations. *In* Methods in Neuronal Modeling. C. Koch and I. Segev, editors. MIT press, Cambridge, MA. 135–169.

Rose, R. M., and J. L. Hindmarsh. 1989. The assembly of ionic currents in a thalamic neuron. I. The three-dimensional model. *Proc. R. Soc. Lond. B Biol. Sci.* 237:267–288.

Schwindt, P. C., W. J. Spain, and W. E. Crill. 1992. Effects of intracellular calcium chelation on voltage-dependent and calcium-dependent currents

in cat neocortical neurons. *Neuroscience.* 47:571–578.

Soltesz, I., S. Lightowler, N. Leresche, D. Jassik-Gerschenfeld, C. E. Pol-lard, and V. Crunelli. 1991. Two inward currents and the transformation of low frequency oscillations of rat and cat thalamocortical cells. *J. Physiol. (Lond.).* 441:175–197.

Steriade, M., and M. Deschênes. 1984. The thalamus as a neuronal oscillator. *Brain Res. Rev.* 8:1–63.

Steriade, M., and R. R. Llinas. 1988. The functional states of the thalamus and the associated neuronal interplay. *Physiol. Rev.* 68:649–742.

Steriade, M., M. Deschênes, L. Domich, and C. Mulle. 1985. Abolition of spindle oscillations in thalamic neurons disconnected from nucleus re-ticularis thalami. *J. Neurophysiol.* 54:1473–1497.

Steriade, M., L. Domich, G. Oakson, and M. Deschênes. 1987. The deaf-ferented reticular thalamic nucleus generates spindle rhythmicity. *J. Neu-rophysiol.* 57:260–273.

Steriade, M., P. Gloor, R. R. Llinas, F. H. Lopes da Silva, and M. M. Me-sulam. 1990. Basic mechanisms of cerebral rhythmic activities. *EEG Clin. Neurophysiol.* 76:481–508.

Steriade, M., E. G. Jones, and R. R. Llinas. 1990. Thalamic Oscillations and Signalling. John Wiley & Sons, New York. 431 pp.

Steriade, M., D. Contreras, R. Currό Dossi, and A. Nunez. 1993a. The slow (<1 Hz) oscillation in reticular thalamus and thalamocortical neurons. Scenario of sleep rhythms generation in interacting thalamic and neo-cortical networks. *Neuroscience.* 13:3284–3299.

Steriade, M., D. A. McCormick, and T. J. Sejnowski. 1993b. Thalamocor-tical oscillations in the sleeping and aroused brain. *Science (Wash. DC).* In press.

Toth, T., and V. Crunelli. 1992a. Computer simulations of the pacemaker oscillations of thalamocortical cells. *NeuroReport.* 3:65–68.

Toth, T., and V. Crunelli. 1992b. Modelling spindle-like oscillations in thala-mocortical neurones. *Soc. Neurosci. Abstr.* 18:1018.

Traub, R. D., and R. Miles. 1991. Neuronal Networks of the Hippocampus. Cambridge University Press, Cambridge. 281 pp.

Uchimura, N., E. Cherubini, and R. A. North. 1990. Cation current activated by hyperpolarization in a subset of rat nucleus accumbens neurons. *J. Neurophysiol.* 64:1847–1850.

van Ginneken, A. C. G., and W. Giles. 1991. Voltage-clamp measurements of the hyperpolarization-activated inward current I_f in single cells from rabbit sino-atrial node. *J. Physiol. (Lond.).* 434:57–83.

von Krosigk, M., T. Bal, and D. A. McCormick. 1993. Cellular mechanisms of a synchronized oscillation in the thalamus. *Science (Wash. DC).* 261: 361–364.

Wang, X. J., J. Rinzel, and M. A. Rogawski. 1991. A model of the T-type calcium current and the low-threshold spike in thalamic neurons. *J. Neu-rophysiol.* 66:839–850.

Zeeman, E. C. 1973. Differential equations for the heart beat and nerve impulse. *In* Dynamical Systems. M. Peixoto, editor. Academic Press, New York. 683–741.